THE JOURNAL OF PHYSICAL CHEMISTRY C

Article

pubs.acs.org/JPCC

Ionization Energy as a Stability Criterion for Halide Perovskites

Chao Zheng* and Oleg Rubel*

Department of Materials Science and Engineering, McMaster University, Hamilton, Ontario L8S 4L8, Canada

ABSTRACT: Instability of hybrid organic–inorganic halide perovskites hinders their development for photovoltaic applications. First-principles calculations are used for evaluation of a decomposition reaction enthalpy of hybrid halide perovskites, which is linked to experimentally observed degradation of device characteristics. However, simple criteria for predicting the intrinsic stability of halide perovskites are lacking since Goldschmidt's tolerance and octahedral geometrical factors do not fully capture formability of those perovskites. In this paper, we extend the Born–Haber cycle to partition the reaction enthalpy of various perovskite structures into lattice, ionization, and molecularization energy components. The analysis of various contributions to the reaction enthalpy points to an ionization energy of an organic molecule and an inorganic complex ion as an additional criterion for predicting chemical trends in stability of hybrid halide perovskites. The ionization energy equal to or less than that for cesium *and* the size comparable to that of methylammonium define the design space for cations A^+ in the search for new perovskite structures $APbI_3$ with improved chemical stability that are suitable for photovoltaic applications.

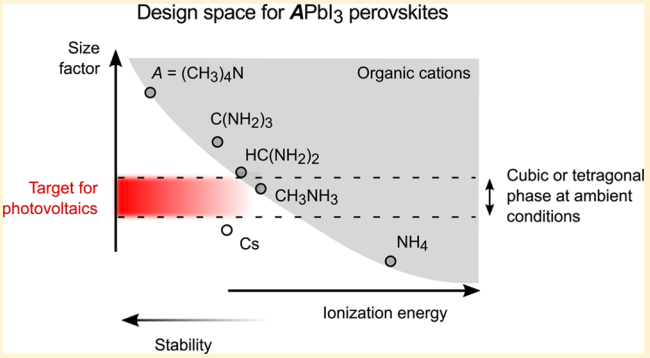

INTRODUCTION

The efficiencies of hybrid organic–inorganic perovskite solar cells have already increased to over 20%.[1−4] Fabrication of hybrid organic perovksite is based on a low temperature solution method, thus offering a low-cost alternative to crystalline thin-film photovoltaic devices. The main obstacle hindering the commercialization of hybrid organic perovskite solar cells is the instability of the active material. Hybrid perovskites are prone to a phase separation that takes place instantly under the ambient environment (moisture, UV radiation, atmospheric oxygen, etc.).[5−7] The detrimental role of moisture in creating a degradation pathway for halide perovskites was previously discussed from acid–base chemistry,[8] molecular dynamic simulations,[9,10] hydrolysis reaction,[11] and thermodynamic[12] perspectives. Encapsulation of the perovskite cells does not prevent their degradation either. The active layer of encapsulated hybrid organic perovskites eventually decomposes after a period of time that ranges from several days to a month.[13,14]

Intrinsic instability of hybrid halide perovskite structures can be captured at the level of first-principles calculations[15−17] by evaluating the enthalpy of the reaction

$$AX + BX_2 \rightarrow ABX_3 \quad (1)$$

based on the total energy of the solid compounds involved. Here, A represents an organic cation, B and X are the metal and halide elements, respectively. The negative reaction enthalpy ΔH_r indicates stable products. The lower the value of ΔH_r, the more stable the structure is against decomposition. For example, the reaction enthalpy for tetragonal $CH_3NH_3PbI_3$ is within the range of −0.1 to 0.06 eV per formula unit,[7,12,15] which renders the structure to be at the boundary between weakly stable and unstable, agreeing with experimental observations.[7] Despite the success of first-principles calculations in predicting formability of hybrid halide perovskite structures, the origin of intrinsic instability and avenues for its improvement remain unclear.

Geometrical factors such as the Goldschmidt's tolerance factor[18] and octahedral factor successfully explain the formability of various inorganic perovskite structures.[19] The tolerance factor t measures compactness of the perovskite structure. The value of the tolerance factor for $CH_3NH_3PbI_3$ is t = 0.91,[20] which is within the range of acceptable values t = 0.8–0.95.[19] Li et al.[19] pointed out that the tolerance factor alone does not fully capture the formability of perovkite structures and proposed to add Pauling's octahedral factor[21] r_B/r_X (r_B and r_X are the ionic radii of cation B and anion X, respectively) as an additional geometrical criterion. In the case of $CH_3NH_3PbI_3$, the octahedral factor r_{Pb}/r_I = 0.54 is within the allowable range of 0.414–0.732.[21] This analysis suggests that geometrical factors are not sufficient to explain the instability of hybrid halide perovskites.

Frost et al.[8] attributed the instability of hybrid organic halide perovskites to a relatively low electrostatic lattice energy of their ionic structure as compared to non-halide perovskite compounds. For instance, traditional inorganic perovskites of the II–IV–VI_3 family, e.g., $PbTiO_3$, have the lattice energy of −119 eV. This value is much lower that the lattice energy of

Received: January 11, 2017
Revised: May 12, 2017
Published: May 12, 2017

DOI: 10.1021/acs.jpcc.7b00333
J. Phys. Chem. C 2017, 121, 11977–11984

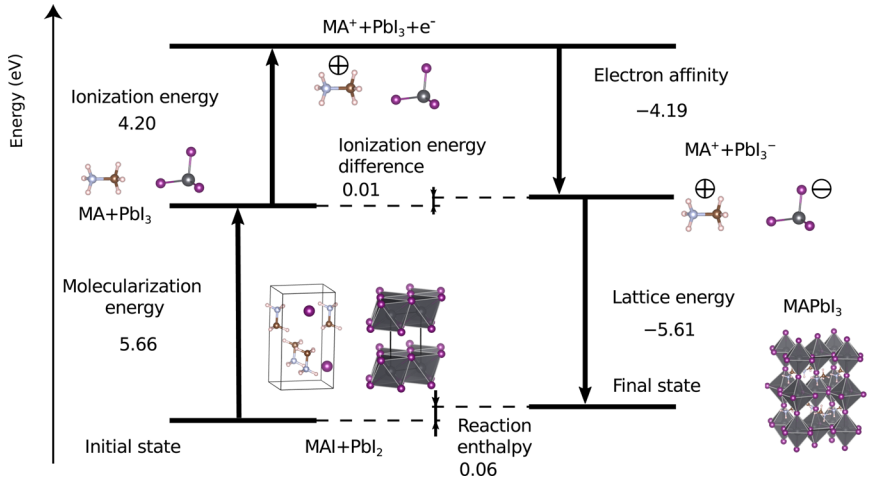

Figure 1. Born−Haber cycle of methylammonium (MA) lead iodide obtained with $[CH_3NH_3]^+$ and $[PbI_3]^-$ ions as elementary species.

−28 eV for $CH_3NH_3PbI_3$ perovksite, which belongs to the I−II−VII_3 family. This argument suggests that I−II−VII_3 perovskites have intrinsically lower electrostatic energy and thus weaker chemical stability. On the other hand, the experimental reaction enthalpy for $PbTiO_3$ is only −0.38 eV,[22] which is orders of magnitude less than its lattice energy. It is also known that the $CsPbI_3$ perovskite structure is indeed stable up to the temperature of 460 °C,[23] above which the material melts without decomposition, despite its higher lattice energy of −27 eV. These observations indicate that the lattice energy alone cannot be used as a criterion for stability of ionic structures.

The Born−Haber cycle is traditionally used for analysis of formation enthalpies. It allows one to break the formation energy into the following components: atomization enthalpy, ionization enthalpy, and lattice enthalpy.[24] In this paper, we extend the Born−Haber cycle to the analysis of energy components of the reaction enthalpies for various perovskite structures using the density functional theory (DFT). It will be shown that, in I−II−VII_3 organic and inorganic perovskites, the lattice energy contribution is largely canceled by the molecularization energy, leaving the ionization enthalpy to determine the direction of the reaction. The instability of hybrid organic lead−iodine perovskites can be attributed to the high energy associated with ionization of organic molecules and $[PbI_3]^-$.

METHODS

Basic Concepts. The Born−Haber cycle was originally proposed by Max Born and Fritz Haber as a way to measure formation energies of ionic structures.[24] The cycle also provides a method to determine the lattice energy of the structures, which otherwise cannot be directly measured experimentally. Here, we will explain the essence of the Born−Haber cycle and its utilization for analysis of reaction enthalpy components using the $CH_3NH_3PbI_3$ perovksite structure as an example.

The formation process of $CH_3NH_3PbI_3$ from solid CH_3NH_3I and PbI_2 compounds can be subdivided into several consecutive steps illustrated in Figure 1. The initial step—molecularization (similar to the atomization in the original Born−Haber cycle)—involves breaking the CH_3NH_3I and PbI_2 lattice structures and formation of CH_3NH_3 and PbI_3 molecules

$$CH_3NH_3I(s) + PbI_2(s) \xrightarrow{\Delta H_{mo}} CH_3NH_3(g) + PbI_3(g) \quad (2)$$

The rational for using CH_3NH_3 and PbI_3 radicals as the smallest units in the Born−Haber cycle is justified by the existence of the corresponding free-standing ions,[25−28] and will be discussed in the next section.

The next step is the ionization of the CH_3NH_3 molecule

$$CH_3NH_3(g) + PbI_3(g) \xrightarrow{\Delta H_{ion,1}} CH_3NH_3^+(g) + PbI_3(g) + e^- \quad (3)$$

followed by the ionization of PbI_3

$$CH_3NH_3^+(g) + PbI_3(g) \xrightarrow{\Delta H_{ion,2}} CH_3NH_3^+(g) + PbI_3^-(g) + e^- \quad (4)$$

It can be seen from the diagram in Figure 1 that the formation of $[CH_3NH_3]^+$ ion is an endothermic process, whereas the ionization of PbI_3 is an exothermic process. The resultant ionization energy is an additive of two enthalphies

$$\Delta H_{ion} = \Delta H_{ion,1} + \Delta H_{ion,2} \quad (5)$$

Finally, electrically charged $[CH_3NH_3]^+$ and $[PbI_3]^-$ complex ions are combined to form $CH_3NH_3PbI_3$ crystalline structure

$$CH_3NH_3^+(g) + PbI_3^-(g) \xrightarrow{\Delta H_{latt}} CH_3NH_3PbI_3(s) \quad (6)$$

The amount of energy ΔH_{latt} released in this reaction is called the lattice energy of the hybrid organic perovskite structure. This concludes the Born−Haber cycle of $CH_3NH_3PbI_3$. The total reaction enthalpy is compiled from enthalpies of individual steps of the cycle

$$\Delta H_r = \Delta H_{mo} + \Delta H_{ion} + \Delta H_{latt} \quad (7)$$

Computational Details. Electronic structure calculations have been performed in the framework of DFT[29] and Perdew−Burke−Ernzerhof generalized gradient approximation[30] (GGA-PBE) for the exchange-correlation functional. Total energies of all compounds were obtained using the Vienna *Ab initio* Simulation Package (VASP) and projector augmented-wave (PAW) potentials.[31−33]

All crystal structures of compounds studied here are taken at their most stable polymorph at ambient conditions. Among perovskite structures, $CH_3NH_3PbI_3$ adapts a tetragonal β-phase at the ambient temperature, $CH_3NH_3PbBr_3$ and $CH_3NH_3PbCl_3$

DOI: 10.1021/acs.jpcc.7b00333
J. Phys. Chem. C 2017, 121, 11977−11984

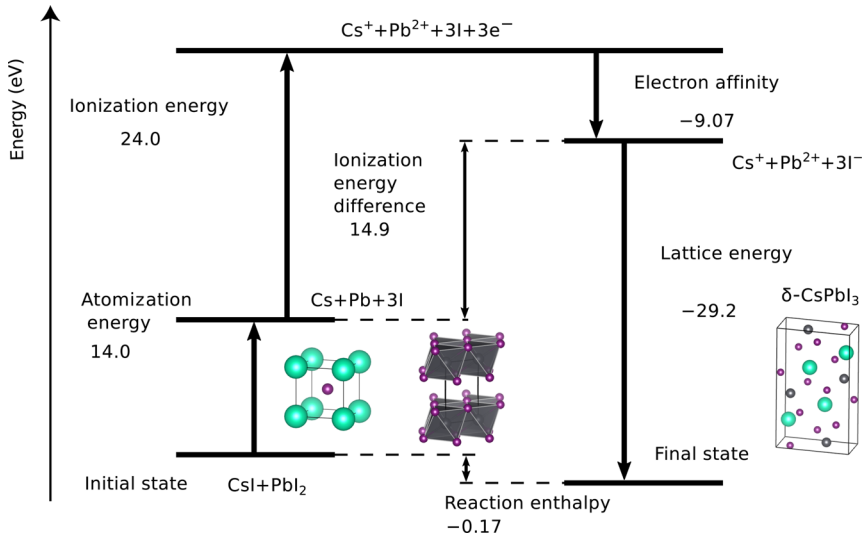

Figure 2. Born−Haber cycle of cesium lead iodide obtained with Cs^+, Pb^{2+}, and I^- ions as elementary species.

have a cubic phase,[34,35] and $C(NH_2)_3PbI_3$ and $(CH_3)_4NPbI_3$ favor hexagonal structures.[36−38] $HC(NH_2)_2PbI_3$ adopts a hexagonal δ-phase.[39] $CsPbI_3$, $CsPbBr_3$, and $CsPbCl_3$ prefer an orthorhombic (*Pnma*) δ-phase.[23,40] The crystal structures of CH_3NH_3I, CH_3NH_3Br, and CH_3NH_3Cl organic salts correspond to α'-tetragonal (*P4/nmm*) phase at room temperature.[41−43] Szafrański and Jarek[44] reported the structures of guanidinium iodide $C(NH_2)_3I$, and the structure of tetramethylammonium iodine $(CH_3)_4NI$ was obtained using $(CH_3)_4NAu$[45] as a parent structure, followed by full relaxation of their structural parameters. The structure of $HC(NH_2)_2I$ was obtained from orthorhombic (*Pbca*) $C(NH_2)_3Cl$[46] with full relaxation of the structural parameters. Cubic crystal structures of CsI, CsBr, CsCl, and NaCl as well as hexagonal PbI_2 and orthorhombic $PbBr_2$ were taken from Wyckoff[47] and Gerlach.[48] The crystal structure of orthorhombic $PbCl_2$ was derived from the structure of $PbBr_2$. Crystallographic information files (CIFs) with atomic structures used in calculations can be accessed through the Cambridge Crystallographic Data Centre (CCDC deposition numbers 1549654−1549681).

For reciprocal space integration, a 4 × 4 × 4 Monkhorst−Pack grid[49] was used for cubic phases, 3 × 3 × 2 was used for tetragonal phases, 4 × 4 × 3 for hexagonal phases, 3 × 6 × 2 for orthorhombic $CsPbX_3$ phases, and 4 × 8 × 4 for orthorhombic $PbBr_2$ and $PbCl_2$. The convergence of reaction enthalpies with respect to the *k*-mesh density is better than 5 meV, which was tested by doubling the density for several perovskite structures and their parent compounds. The cutoff energy for a plane-wave expansion was set at 400 eV. The lattice constant and atomic positions were optimized such that residual forces acting on atoms did not exceed 2 meV/Å, and the residual hydrostatic pressure was less than 50 MPa.

Gaseous phases, such as Cs, $[CH_3NH_3]^+$, and $[PbI_3]^-$, were modeled as an individual atom/molecule surrounded by 20 Å of vacuum. All calculations related to gaseous phases were performed in conjunction with optimization of internal degrees of freedom. Only the Γ-point was used in the Brillouin zone. The ionization energy of positively charged ions was calculated by subtracting the total energy of cations (e.g., Cs^+, $[CH_3NH_3]^+$, $[C(NH_2)_3]^+$) from the energy of neutral atoms or molecules (e.g., Cs, CH_3NH_3, $C(NH_2)_3$). Similarly, the electron affinity of negatively charged ions was modeled by adding one electron to $PbCl_3$, $PbBr_3$, or PbI_3 molecules to form $[PbCl_3]^-$, $[PbBr_3]^-$, and $[PbI_3]^-$ anions. The electron affinity of these ions was represented as an energy difference between negatively charged complex ions and neutral species. Monopole, dipole, and quadrupole corrections implemented in VASP[50,51] were used for eliminating leading errors and acquiring accurate total energies of all charged ions.

VESTA 3 package[52] was used to visualize crystal structures and for computing the Madelung electrostatic energy using oxidation state as formal charges. In these calculations, the radius of the ionic sphere and the reciprocal-space range were set at 1 Å and 4 $Å^{-1}$, respectively.

RESULTS AND DISCUSSION

Lattice Energies of Halide Perovskites. Calculation of individual energies associated with various steps in the Born−Haber cycle requires subdivision of the ionic solid in question into elementary species. In the case of alkali halides (such as NaCl, CsCl, etc.), the atomization is an apparent choice. Following the same strategy, Cs^+, Pb^{2+}, and I^- ions can be used to calculate the lattice energy, which yields $\Delta H_{latt} \simeq -29$ eV (Figure 2).

This value agrees well with the Madelung energy of −27 eV obtained from the point charge model. Gopal[53] noticed the existence of a trend between the lattice energy ΔH_{latt} and the melting point T_m of alkali halides with the proportionality factor of $-\Delta H_{latt}/T_m \approx 7.4 \times 10^{-3}$ eV/K. Assuming that the same proportionality holds for perovskite structures, the melting point of I−II−VII_3 perovskites would be near 3900 K, which is an order of magnitude greater than the actual values of 733−888 K for group-I lead halide perovskites ($CsPbI_3$, $CsPbBr_3$, and $CsPbCl_3$).[54,55]

Alternatively, we can separate the $CsPbI_3$ perovskite structure into two ions Cs^+ and $[PbI_3]^-$. The existence of the corresponding free-standing ions was verified experimentally.[25,26] Using this approach, we re-evaluated the lattice energy of $CsPbI_3$ as −5.55 eV using the Born−Haber cycle similar to that shown in Figure 1. This result translates into a substantially lower melting point of approximately 750 K, which is remarkably close to the experimental value of 749 K.

Similar calculations of the lattice energy were performed for other inorganic I−II−VII_3 and II−IV−VI_3 perovksites. Results

DOI: 10.1021/acs.jpcc.7b00333
J. Phys. Chem. C 2017, 121, 11977−11984

Table 1. Components (eV) of the Reaction Enthalpies Extracted from Born−Haber Cycle as Well as the Melting Temperature and Stability against Spontaneous Decomposition for Halide Perovskites and Other Ionic Structures

compounds	ΔH_{mo}	ΔH_{latt}	ΔH_{ion}	ΔH_r	T_m (K)	stability[a]
δ-$CsPbCl_3$	6.23	−5.95	−0.67	−0.39	888[55]	Y[23]
δ-$CsPbBr_3$	5.80	−5.72	−0.46	−0.39	840[54]	Y[23]
δ-$CsPbI_3$	5.72	−5.55	−0.34	−0.17	749[23]	Y[23]
$CH_3NH_3PbCl_3$	6.20	−6.03	−0.32	−0.15		Y[7]
$CH_3NH_3PbBr_3$	5.80	−5.81	−0.11	−0.11		Y[7]
β-$CH_3NH_3PbI_3$	5.66	−5.61	0.01	0.06		N[7]
δ-$HC(NH_2)_2PbI_3$	5.40	−5.47	−0.23	−0.29		Y[39]
$C(NH_2)_3PbI_3$	5.43	−5.43	−0.38	−0.39		Y[37]
$(CH_3)_4NPbI_3$	5.47	−4.79	−1.05	−0.37		Y[38]
CsCl	2.59	−6.64	0.14	−3.91	918[56]	Y
NaCl[b]	3.01	−8.22	1.46	−3.76	1077[57]	Y

[a]Stability data here are from experiments: "Y" refers to materials that do not undergo spontaneous phase separation at the room temperature (excluding environmental factors, such as moisture, oxygen, UV light). [b]Experimental values for NaCl:[24] ΔH_{mo} = 2.37 eV, ΔH_{latt} = −8.15 eV, ΔH_{ion} = 1.52 eV, ΔH_r = −4.26 eV.

are summarized in Table 1. NaCl was used as a benchmark for comparison between calculated and experimental components of the formation enthalpy. The agreement with experimental values gives a confidence in the approach used. The discrepancy in ΔH_{mo} can be attributed to the use of non-spin-polarized calculations for individual atoms and ions. The plot of the melting point vs the lattice energy of those compounds is shown in Figure 3. From this figure, we can see that the melting

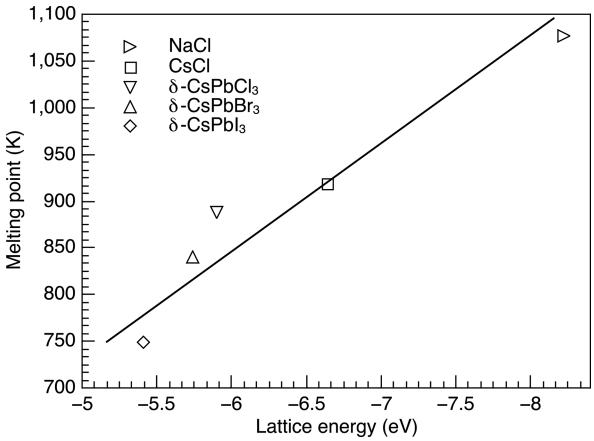

Figure 3. Correlation between the lattice energy and melting temperature of ionic compounds. The line is a guide to the eye.

point of different ionic structures including alkali halides follows a linear trend line. This suggests that that formation of A^+ cations and $[BX_3]^-$ complex anions is a plausible scenario during melting of the perovskite structures.

Stability Analysis of Hybrid Organic Halide Perovksites. Now we will utilize the Born−Haber cycle in order to evaluate components of the reaction enthalpy of hybrid halide perovskits. The lattice energies of $CH_3NH_3PbCl_3$, $CH_3NH_3PbBr_3$, and β-$CH_3NH_3PbI_3$ perovskites are listed in Table 1. All three compounds have similar values of the lattice energies (~10% max−min difference). However, their stability characteristics are quite different. Buin et al.[7] demonstrated that, under ambient conditions, $CH_3NH_3PbCl_3$ and $CH_3NH_3PbBr_3$ do not undergo a spontaneous phase separation, unlike β-$CH_3NH_3PbI_3$. Both $CH_3NH_3PbCl_3$ and $CH_3NH_3PbBr_3$ remain stable up to the temperature of approximately 520 K, above which they decompose.[20] Lattice energies of the corresponding inorganic perovskites ($CsPbI_3$, $CsPbBr_3$, and $CsPbCl_3$) are very similar to their organic counterparts. In fact, these inorganic perovskites are chemically stable under the ambient environment. Remarkably, the lattice energies of β-$CH_3NH_3PbI_3$ and δ-$CsPbCl_3$ structures are identical, in spite of the distinct stability characteristics. Therefore, we can conclude that the lattice energy cannot be used as a criterion to predict the chemical stability of compounds.

The analysis of various contributions to the reaction enthalpies of hybrid halide perovskites (Table 1) shows that the molecularization and lattice energies largely cancel each other. The molecularization energy in reaction 2 is largely governed by the methylammonium iodide bond strength as evident from Figure 4. The energy consumed to separate

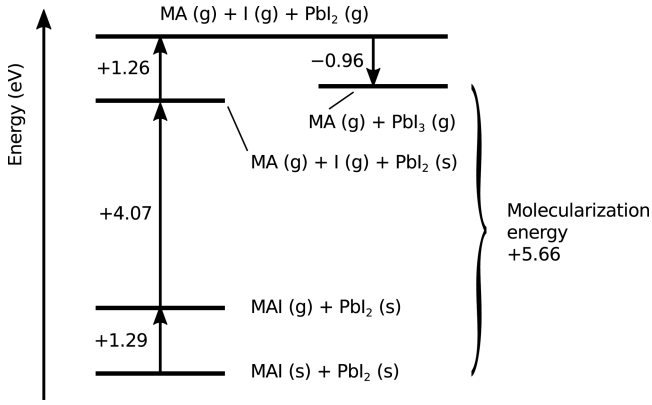

Figure 4. Components of the molecularization energy in the reaction 2. MA stands for the methylammonium CH_3NH_3.

$PbI_2(s)$ to $PbI_2(g)$ and the energy gained from adding an I atom to $PbI_2(g)$ to form $PbI_3(g)$ roughly cancel each other. We estimated the Madelung energy of CH_3NH_3I to be −6.8 eV/f.u. by placing $+1e$ and $-1e$ on the nitrogen and iodine atoms, respectively. This lattice energy of CH_3NH_3I includes −1 eV/f.u. associated with the ionization energy of I^- and $[CH_3NH_3]^+$. Therefore, the lattice energy of $CH_3NH_3PbI_3$, −5.61 eV/f.u. (Table 1), is inherited from the lattice energy of the parent salt, CH_3NH_3I.

The ionization energy of $[CH_3NH_3]^+$ and $[PbI_3]^-$ is the remaining contribution to the reaction enthalpy in eq 7 that

DOI: 10.1021/acs.jpcc.7b00333
J. Phys. Chem. C 2017, 121, 11977−11984

ultimately controls the balance of the reaction. The lower ΔH_{ion} is, the more stable the compound.

Let us examine the chemical trends in ionization energy of various perovskites. The total ionization energy (eq 5) comprises two components: the ionization energy for the cation (Cs^+ or $[CH_3NH_3]^+$) and that for the complex ion ($[PbI_3]^-$, $[PbBr_3]^-$, or $[PbCl_3]^-$). Cesium has a lower ionization energy than CH_3NH_3 (Table 2), which explains trends in the higher chemical stability of Cs-based perovskites as compared to their CH_3NH_3-based counterparts.

Table 2. Ionization Energies (eV) of Atoms and Molecules Calculated with DFT[c]

ions	$\Delta H_{ion,1/2}$
$[(CH_3)_4N]^+$	3.15
$[C(NH_2)_3]^+$	3.81
Cs^+	3.85
$[HC(NH_2)_2]^+$	3.97
$[CH_3NH_3]^+$	4.20
$[NH_4]^+$	4.78
Na^+	5.17[a]
$[CH_3PH_3]^+$	5.20
$[CH_3SH_2]^+$	5.30
$[PH_4]^+$	5.36
$[HCNH_2PH_2]^+$	8.36
$[CH_3]^+$	10.0[b]
$[PbCl_3]^-$	−4.52
$[PbBr_3]^-$	−4.31
$[PbI_3]^-$	−4.19

[a]5.20 eV experimental ionization energy.[24] [b]9.84 eV experimental ionization energy.[58,59] [c]Lower values favor formability of perovskites.

Switching halides in the complex ions from PbI_3 to $PbCl_3$ lowers their electron affinity (Table 2) and, thus, leads to the lower total ionization energy. This explains the increase of the chemical stability when changing the inorganic cage from PbI_3 to $PbBr_3$ and $PbCl_3$ as illustrated in Figure 5.

In order to achieve chemically stable hybrid halide perovskite structures, the necessary requirements are favorable geometrical factors (*t*-factor and octahedral factor) in conjunction with the low ionization energy ($\Delta H_{ion} \lesssim 0$ eV). Two strategies can be used to achieve this goal: (i) find a cation with the low ionization energy or (ii) select an inorganic cage with the low electron affinity. The second avenue is not very promising, since the band gap of $PbBr_3$- and $PbCl_3$-based hybrid perovskites (2.3 eV[60] and 2.9 eV,[61] respectively) is outside of the favorable range for single-junction solar cells.

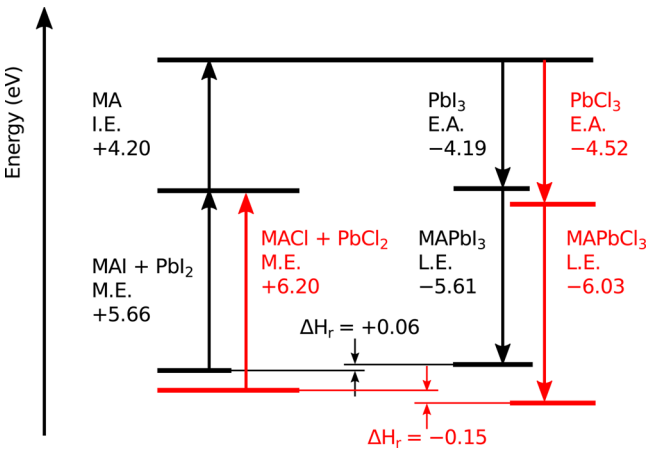

Figure 5. Influence of halide element on the Born−Haber cycle of hybrid halide perovskites. A comparison between $CH_3NH_3PbI_3$ and $CH_3NH_3PbCl_3$. The following components are shown: the molecularization energy (M.E.), the ionization energy (I.E.), the electron affinity (E.A.), and the lattice energy (L.E.).

Since cesium has the lowest ionization energy in the periodic table, it is a challenging task to find molecules with smaller or similar ionization energy. Among the variety of organic cations listed in the Table 2, $[C(NH_2)_3]^+$, $[HC(NH_2)_2]^+$, and $[(CH_3)_4N]^+$ have the ionization energies lower than that for $[CH_3NH_3]^+$ cation, making them favorable candidates for perovskites with improved stability. However, the size of $C(NH_2)_3$, $HC(NH_2)_2$, and $(CH_3)_4N$ molecules is significantly greater than CH_3NH_3, which raises the tolerance factor above the upper formability limit of 0.95 (Table 3).

Table 3. Size of Organic Cations, the Tolerance Factor, Volume of the Unit Cell, and the Band Gap of Selected Perovskites

perovskite	cation radius (pm)	tolerance factor[38,62]	volume (Å^3/f.u.)	band gap (eV)
β-$CH_3NH_3PbI_3$	217[38,62]	0.91	262	1.62
δ-$HC(NH_2)_2PbI_3$	253[38]	0.99	313	3.26
$C(NH_2)_3PbI_3$	278[38,62]	1.04	326	3.38
$(CH_3)_4NPbI_3$	320[63,64]	1.15	361	3.30

The structures $C(NH_2)_3PbI_3$, $HC(NH_2)_2PbI_3$, and $(CH_3)_4NPbI_3$ show favorable reaction enthalpies of −0.39, −0.29, and −0.37 eV, respectively (Table 1). A large size of the organic molecule hinders formability of $C(NH_2)_3PbI_3$, $HC(NH_2)_2PbI_3$, and $(CH_3)_4NPbI_3$ perovksite structures in the cubic or tetragonal phases. They all adapt a hexagonal structure at ambient temperature.[37−39] However, this phase tends to have a wider band gap, which impairs its prospects for use in photovoltaic applications. Nevertheless, we discuss the link between our calculations and experimental evidence for stability of $C(NH_2)_3PbI_3$, $HC(NH_2)_2PbI_3$, and $(CH_3)_4NPbI_3$ compounds.

Marco et al.[65] successfully synthesized and characterized $C(NH_2)_3PbI_3$ perovskite solar cells. It was found that the power conversion efficiency of the $C(NH_2)_3PbI_3$ solar cell degrades over time. Interestingly, the rate of the efficiency decay is slower for $C(NH_2)_3PbI_3$ as compared to $CH_3NH_3PbI_3$. Szafrański[66] observed that $C(NH_2)_3PbI_3$ crystals transform from orange-reddish phase to yellow phase after several hours at ambient pressure and temperature. The optical bleaching is associated with a phase transformation that yields the hexagonal phase rather than the phase separation.[66] $HC(NH_2)_2PbI_3$ prefers a cubic phase at the high temperature (160 °C) and takes a hexagonal phase at the ambient temperature.[39,67]

The question is if there are any organic cations of the suitable size that fulfill the requirements on the low ionization energy. The ionization energies of onium ions in Table 2 correlate with the proton affinity of the corresponding molecules.[68] Molecules with the low ionization energy exhibit strong proton affinity and *vice versa*. For instance, the proton affinity of PH_3 is 785 kJ/mol, which is much lower than 901 kJ/mol for CH_3NH_2. It turns out that methylamine has one of the strongest proton affinity among organic compounds. There are very few organic molecules (including $(CH_3)_2NH$ studied here) with stronger

DOI: 10.1021/acs.jpcc.7b00333
J. Phys. Chem. C 2017, 121, 11977−11984

proton affinity than CH_3NH_2, but none of them have a size compatible with the PbI_3 cage.

CONCLUSIONS

The Goldschmidt's tolerance and octahedral geometrical factors do not fully capture prerequisites for formability of hybrid halide perovskites. Here, we used DFT calculations in conjunction with a Born−Haber cycle to evaluate contributions of the lattice, ionization, and molecularization energies to the decomposition reaction enthalpy of hybrid halide perovskites. It was previously assumed that the instability of halide perovskite is due to a lower lattice energy of their ionic structure. We observe a correlation between the lattice energies and melting temperatures, but not with reaction enthalpies that are ultimately linked to the chemical instability of the perovskites. Analysis of the Born−Haber cycle components suggests that the reaction enthalpy of hybrid halide perovskites is governed by the sum of ionization energies of a cation, e.g., $[CH_3NH_3]^+$, and an anion, e.g., $[PbI_3]^-$. The lower total ionization energy, the more stable is the structure, provided the geometrical conditions are fulfilled (the tolerance and octahedral factors). This explains chemical trends in stability of hybrid and inorganic halide perovskites. For instance, the relatively high stability of $CH_3NH_3PbCl_3$ is attributed to a lower ionization energy of the $[PbCl_3]^-$ complex ion, whereas the stability of $CsPbI_3$ is due to the lower ionization energy of Cs^+. The ionization energy of organic cations correlates with their proton affinity. In the search for hybrid perovskite with improved chemical stability and the band gap suitable for photovoltaic applications, several cations were investigated. The promising candidates are $[C(NH_2)_3]^+$, $[HC(NH_2)_2]^+$, and $[(CH_3)_4N]^+$ with the ionization energies even lower than $[CH_3NH_3]^+$. The corresponding $C(NH_2)_3PbI_3$, $HC(NH_2)_2PbI_3$, and $(CH_3)_4NPbI_3$ structures have the decomposition reaction enthalpy that is at least 0.35 eV more favorable than $CH_3NH_3PbI_3$. However, these ions have a prohibitively large size and thus prefer a hexagonal structure that translates into a large band gap (greater than 3 eV). It is the fact that CH_3NH_2 has the highest proton affinity among molecules of comparable size that makes it challenging to find a cation suitable for the PbI_3 cage.

Our calculations do not include environmental factors, such as degradation in water or oxidation in air. However, the reaction enthalpy determines a saturation concentration of $[CH_3NH_3]^+$ ions during dissolution of $CH_3NH_3PbI_3$ in water.[12] Therefore, improvement in the reaction enthalpy will also enhance the stability of perovskite structures in the moist environment.

AUTHOR INFORMATION

Corresponding Authors

*E-mail: zhengc8@mcmaster.ca. Phone: +1647-936-1436 (C.Z.).

*E-mail: rubelo@mcmaster.ca. Phone: +1905-525-9140, ext. 24094 (O.R.).

ORCID

Chao Zheng: 0000-0001-5441-6720

Oleg Rubel: 0000-0001-5104-5602

Notes

The authors declare no competing financial interest.

ACKNOWLEDGMENTS

Funding was provided by the Natural Sciences and Engineering Research Council of Canada under the Discovery Grant Program RGPIN-2015-04518. The work was performed using computational resources of the Thunder Bay Regional Research Institute, Lakehead University, and Compute Canada (Calcul Quebec).

REFERENCES

(1) Lee, M. M.; Teuscher, J.; Miyasaka, T.; Murakami, T. N.; Snaith, H. J. Efficient Hybrid Solar Cells Based on Meso-Superstructured Organometal Halide Perovskites. *Science* **2012**, *338*, 643−647.

(2) Park, N.-G. Organometal Perovskite Light Absorbers Toward a 20% Efficiency Low-Cost Solid-State Mesoscopic Solar Cell. *J. Phys. Chem. Lett.* **2013**, *4*, 2423−2429.

(3) Jung, H. S.; Park, N.-G. Perovskite Solar Cells: From Materials to Devices. *Small* **2015**, *11*, 10−25.

(4) Yang, W. S.; Noh, J. H.; Jeon, N. J.; Kim, Y. C.; Ryu, S.; Seo, J.; Seok, S. I. High-Performance Photovoltaic Perovskite Layers Fabricated Through Intramolecular Exchange. *Science* **2015**, *348*, 1234−1237.

(5) Christians, J. A.; Herrera, P. A. M.; Kamat, P. V. Transformation of the Excited State and Photovoltaic Efficiency of $CH_3NH_3PbI_3$ Perovskite upon Controlled Exposure to Humidified Air. *J. Am. Chem. Soc.* **2015**, *137*, 1530−1538.

(6) Wozny, S.; Yang, M.; Nardes, A. M.; Mercado, C. C.; Ferrere, S.; Reese, M. O.; Zhou, W.; Zhu, K. Controlled Humidity Study on the Formation of Higher Efficiency Formamidinium Lead Triiodide-Based Solar Cells. *Chem. Mater.* **2015**, *27*, 4814−4820.

(7) Buin, A.; Comin, R.; Xu, J.; Ip, A. H.; Sargent, E. H. Halide-Dependent Electronic Structure of Organolead Perovskite Materials. *Chem. Mater.* **2015**, *27*, 4405−4412.

(8) Frost, J. M.; Butler, K. T.; Brivio, F.; Hendon, C. H.; Van Schilfgaarde, M.; Walsh, A. Atomistic Origins of High-Performance in Hybrid Halide Perovskite Solar Cells. *Nano Lett.* **2014**, *14*, 2584−2590.

(9) Mosconi, E.; Azpiroz, J. M.; De Angelis, F. Ab Initio Molecular Dynamics Simulations of Methylammonium Lead Iodide Perovskite Degradation by Water. *Chem. Mater.* **2015**, *27*, 4885−4892.

(10) Zhang, L.; Sit, P. H.-L. Ab Initio Study of Interaction of Water, Hydroxyl Radicals, and Hydroxide Ions with $CH_3NH_3PbI_3$ and $CH_3NH_3PbBr_3$ Surfaces. *J. Phys. Chem. C* **2015**, *119*, 22370−22378.

(11) Zhao, J.; Cai, B.; Luo, Z.; Dong, Y.; Zhang, Y.; Xu, H.; Hong, B.; Yang, Y.; Li, L.; Zhang, e. a.; Gao, C. Wenhua Investigation of the Hydrolysis of Perovskite Organometallic Halide $CH_3NH_3PbI_3$ in Humidity Environment. *Sci. Rep.* **2016**, *6*, 21976.

(12) Tenuta, E.; Zheng, C.; Rubel, O. Thermodynamic Origin of Instability in Hybrid Halide Perovskites. *Sci. Rep.* **2016**, *6*, 37654.

(13) Burschka, J.; Pellet, N.; Moon, S.-J.; Humphry-Baker, R.; Gao, P.; Nazeeruddin, M. K.; Grätzel, M. Sequential Deposition as a Route to High-Performance Perovskite-Sensitized Solar Cells. *Nature* **2013**, *499*, 316−319.

(14) Han, Y.; Meyer, S.; Dkhissi, Y.; Weber, K.; Pringle, J. M.; Bach, U.; Spiccia, L.; Cheng, Y.-B. Degradation Observations of Encapsulated Planar $CH_3NH_3PbI_3$ Perovskite Solar Cells at High Temperatures and Humidity. *J. Mater. Chem. A* **2015**, *3*, 8139−8147.

(15) Zhang, Y.-Y.; Chen, S.; Xu, P.; Xiang, H.; Gong, X.-G.; Walsh, A.; Wei, S.-H. Intrinsic Instability of the Hybrid Halide Perovskite Semiconductor $CH_3NH_3PbI_3$. **2015**, arXiv:1506.01301 arXiv. arXiv.org e-Print archive.

(16) Ganose, A. M.; Savory, C. N.; Scanlon, D. O. $(CH_3NH_3)_2Pb(SCN)_2I_2$: A More Stable Structural Motif for Hybrid Halide Photovoltaics? *J. Phys. Chem. Lett.* **2015**, *6*, 4594−4598.

(17) El-Mellouhi, F.; Bentria, E. T.; Rashkeev, S. N.; Kais, S.; Alharbi, F. H. Enhancing Intrinsic Stability of Hybrid Perovskite Solar Cell by Strong, yet Balanced, Electronic Coupling. *Sci. Rep.* **2016**, *6*, 30305.

(18) Goldschmidt, V. M. Die Gesetze der Krystallochemie. *Naturwissenschaften* **1926**, *14*, 477−485.

DOI: 10.1021/acs.jpcc.7b00333
J. Phys. Chem. C 2017, 121, 11977−11984

(19) Li, C.; Soh, K. C. K.; Wu, P. Formability of ABO_3 Perovskites. *J. Alloys Compd.* **2004**, *372*, 40−48.
(20) Nagabhushana, G.; Shivaramaiah, R.; Navrotsky, A. Direct Calorimetric Verification of Thermodynamic Instability of Lead Halide Hybrid Perovskites. *Proc. Natl. Acad. Sci. U. S. A.* **2016**, *113*, 7717−7721.
(21) Pauling, L. The Principles Determining the Structure of Complex Ionic Crystals. *J. Am. Chem. Soc.* **1929**, *51*, 1010−1026.
(22) Rane, M. V.; Navrotsky, A.; Rossetti, G. A. Enthalpies of Formation of Lead Zirconate Titanate (PZT) Solid Solutions. *J. Solid State Chem.* **2001**, *161*, 402−409.
(23) Sharma, S.; Weiden, N.; Weiss, A. Phase Diagrams of Quasibinary Systems of the Type: ABX_3−$A'BX_3$; ABX_3−$AB'X_3$, and ABX_3−ABX'_3; X = Halogen. *Z. Phys. Chem.* **1992**, *175*, 63−80.
(24) Treptow, R. S. Determination of ΔH for Reactions of the Born-Haber Cycle. *J. Chem. Educ.* **1997**, *74*, 919.
(25) Cremaschi, P.; Simonetta, M. Barmer to Internal Rotation in the Methylammonium Ion. *J. Mol. Struct.* **1975**, *29*, 39−45.
(26) Lanford, O. E.; Kiehl, S. J. The Solubility of Lead Iodide in Solutions of Potassium Iodide-Complex Lead Iodide Ions. *J. Am. Chem. Soc.* **1941**, *63*, 667−669.
(27) Jeon, S.-J.; Raksit, A. B.; Gellene, G. I.; Porter, R. F. Formation of Hypervalent Ammoniated Radicals by Neutralized Ion Beam Techniques. *J. Am. Chem. Soc.* **1985**, *107*, 4129−4133.
(28) Luo, Y.-R. *Comprehensive Handbook of Chemical Bond Energies*; CRC Press: Boca Raton, FL, 2007; p 152.
(29) Kohn, W.; Sham, L. J. Self-Consistent Equations including Exchange and Correlation Effects. *Phys. Rev.* **1965**, *140*, A1133.
(30) Perdew, J. P.; Burke, K.; Ernzerhof, M. Generalized Gradient Approximation Made Simple. *Phys. Rev. Lett.* **1996**, *77*, 3865.
(31) Kresse, G.; Furthmüller, J. Efficient Iterative Schemes for Ab Initio Total-Energy Calculations Using a Plane-Wave Basis Set. *Phys. Rev. B: Condens. Matter Mater. Phys.* **1996**, *54*, 11169.
(32) Kresse, G.; Joubert, D. From Ultrasoft Pseudopotentials to the Projector Augmented-Wave Method. *Phys. Rev. B: Condens. Matter Mater. Phys.* **1999**, *59*, 1758.
(33) Blöchl, P. Projector Augmented-Wave Method. *Phys. Rev. B: Condens. Matter Mater. Phys.* **1994**, *50*, 17953.
(34) Poglitsch, A.; Weber, D. Dynamic Disorder in Methylammoniumtrihalogenoplumbates (II) Observed by Millimeter-Eave Spectroscopy. *J. Chem. Phys.* **1987**, *87*, 6373−6378.
(35) Onoda-Yamamuro, N.; Matsuo, T.; Suga, H. Calorimetric and IR Spectroscopic Studies of Phase Transitions in Methylammonium Trihalogenoplumbates (II). *J. Phys. Chem. Solids* **1990**, *51*, 1383−1395.
(36) Giorgi, G.; Fujisawa, J.-I.; Segawa, H.; Yamashita, K. Organic-Inorganic Hybrid Lead Iodide Perovskite Featuring Zero Dipole Moment Guanidinium Cations: a Theoretical Analysis. *J. Phys. Chem. C* **2015**, *119*, 4694−4701.
(37) Dimesso, L.; Quintilla, A.; Kim, Y.-M.; Lemmer, U.; Jaegermann, W. Investigation of Formamidinium and Guanidinium Lead Tri-Iodide Powders as Precursors for Solar Cells. *Mater. Sci. Eng., B* **2016**, *204*, 27−33.
(38) Liu, G.; Liu, J.; Sun, Z.; Zhang, Z.; Chang, L.; Wang, J.; Tao, X.; Zhang, Q. Thermally Induced Reversible Double Phase Transitions in an Organic-Inorganic Hybrid Iodoplumbate $C_4H_{12}NPbI_3$ with Symmetry Breaking. *Inorg. Chem.* **2016**, *55*, 8025−8030.
(39) Stoumpos, C. C.; Malliakas, C. D.; Kanatzidis, M. G. Semiconducting Tin and Lead Iodide Perovskites with Organic Cations: Phase Transitions, High Mobilities, and Near-infrared Photoluminescent Properties. *Inorg. Chem.* **2013**, *52*, 9019−9038.
(40) Hidaka, M.; Okamoto, Y.; Zikumaru, Y. Structural Phase Transition of $CsPbCl_3$ below Room Temperature. *Phys. Status. Solidi. A* **1983**, *79*, 263−269.
(41) Ishida, H.; Maeda, H.; Hirano, A.; Fujimoto, T.; Kubozono, Y.; Kashino, S.; Emura, S. EXAFS Study on the Phase Transition (Phase α'−δ) in CH_3NH_3I. *Z. Naturforsch., A: Phys. Sci.* **1995**, *50*, 876−880.
(42) Gabe, E. J. The Crystal Structure of Methylammonium Chloride. *Acta Crystallogr.* **1961**, *14*, 1296−1296.
(43) Hughes, E. W.; Lipscomb, W. N. The Crystal Structure of Methylammonium Chloride. *J. Am. Chem. Soc.* **1946**, *68*, 1970−1975.
(44) Szafranski, M.; Jarek, M. Origin of Spontaneous Polarization and Reconstructive Phase Transition in Guanidinium Iodide. *CrystEngComm* **2013**, *15*, 4617−4623.
(45) Dietzel, P. D.; Jansen, M. Synthesis and Crystal Structure Determination of Tetramethylammonium Auride. *Chem. Commun.* **2001**, 2208−2209.
(46) Haas, D.; Harris, D.; Mills, H. The Crystal Structure of Guanidinium Chloride. *Acta Crystallogr.* **1965**, *19*, 676−679.
(47) Wyckoff, R. W. G. *Crystal Structures*; Interscience: New York, 1960; Vol. *2*; pp 85−237.
(48) Gerlach, W. Die Gitterstruktur der Erdalkalioxyde. *Eur. Phys. J. A* **1922**, *9*, 184−192.
(49) Monkhorst, H. J.; Pack, J. D. Special Points for Brillouin-Zone Integrations. *Phys. Rev. B* **1976**, *13*, 5188.
(50) Makov, G.; Payne, M. C. Periodic Boundary Conditions in *Ab Initio* Calculations. *Phys. Rev. B: Condens. Matter Mater. Phys.* **1995**, *51*, 4014−4022.
(51) Neugebauer, J.; Scheffler, M. Adsorbate-Substrate and Adsorbate-Adsorbate Interactions of Na and K Adlayers on Al(111). *Phys. Rev. B: Condens. Matter Mater. Phys.* **1992**, *46*, 16067−16080.
(52) Momma, K.; Izumi, F. VESTA 3 for Three-Dimensional Visualization of Crystal, Volumetric and Morphology Data. *J. Appl. Crystallogr.* **2011**, *44*, 1272−1276.
(53) Gopal, R. Relation Between the Lattice Energy, Melting Point, and Boiling Point of some Crystalline Substances. I. Alkali Halides. *J. Indian Chem. Soc.* **1953**, *30*, 55−58.
(54) Stoumpos, C. C.; Malliakas, C. D.; Peters, J. A.; Liu, Z.; Sebastian, M.; Im, J.; Chasapis, T. C.; Wibowo, A. C.; Chung, D. Y.; Freeman, A. J.; Wessels, B. W.; Kanatzidis, M. G. Crystal Growth of the Perovskite Semiconductor $CsPbBr_3$: A New Material for High-Energy Radiation Detection. *Cryst. Growth Des.* **2013**, *13*, 2722−2727.
(55) Fayon, F.; Vaills, Y.; Simon, P.; Echegut, P.; Bessada, C.; Emery, J.; Buzare, J.-Y. Study of $CsPbCl_3$ between T = 47°C and the Melting Point by the ^{133}Cs NMR and $[Gd_3^+]$ EPR Measurements. *Ferroelectrics* **1996**, *185*, 201−204.
(56) Johnson, J.; Agron, P.; Bredig, M. Molar Volume and Structure of Solid and Molten Cesium Halides. *J. Am. Chem. Soc.* **1955**, *77*, 2734−2737.
(57) Hunter, L. The Variation with Temperature of the Principal Elastic Moduli of NaCl near the Melting Point. *Phys. Rev.* **1942**, *61*, 84.
(58) Reeher, J. R.; Flesch, G. D.; Svec, H. J. The Mass Spectra and Ionization Potentials of the Neutral Fragments Produced During the Electron Bombardment of Aromatic Compounds. *Org. Mass Spectrom.* **1976**, *11*, 154−166.
(59) Berkowitz, J.; Ellison, G. B.; Gutman, D. Three Methods to Measure RH Bond Energies. *J. Phys. Chem.* **1994**, *98*, 2744−2765.
(60) Ryu, S.; Noh, J. H.; Jeon, N. J.; Kim, Y. C.; Yang, W. S.; Seo, J.; Seok, S. I. Voltage Output of Dfficient Perovskite Solar Cells with High Open-Circuit Voltage and Fill Factor. *Energy Environ. Sci.* **2014**, *7*, 2614−2618.
(61) Dimesso, L.; Dimamay, M.; Hamburger, M.; Jaegermann, W. Properties of $CH_3NH_3PbX_3$ (X = I, Br, Cl) Powders as Precursors for Organic/Inorganic Solar Cells. *Chem. Mater.* **2014**, *26*, 6762−6770.
(62) Kieslich, G.; Sun, S.; Cheetham, A. K. Solid-State Principles Applied to Organic-Inorganic Perovskites: New Tricks for an Old Dog. *Chem. Sci.* **2014**, *5*, 4712−4715.
(63) Palomo, J.; Pintauro, P. N. Competitive Absorption of Quaternary Ammonium and Alkali Metal Cations into a Nafion Cation-Exchange Membrane. *J. Membr. Sci.* **2003**, *215*, 103−114.
(64) Garde, S.; Hummer, G.; Paulaitis, M. E. Free Energy of Hydration of a Molecular Ionic Solute: Tetramethylammonium Ion. *J. Chem. Phys.* **1998**, *108*, 1552−1561.
(65) Marco, N. D.; Zhou, H.; Chen, Q.; Sun, P.; Liu, Z.; Meng, L.; Yao, E.-P.; Liu, Y.; Schiffer, A.; Yang, Y. Guanidinium: a Route to Enhanced Carrier Lifetime and Open-Circuit Voltage in Hybrid Perovskite Solar Cells. *Nano Lett.* **2016**, *16*, 1009−1016.

DOI: 10.1021/acs.jpcc.7b00333
J. Phys. Chem. C 2017, 121, 11977−11984

(66) Szafranski, M. Investigation of Phase Instabilities in Guanidinium Halogenoplumbates (II). *Thermochim. Acta* **1997**, *307*, 177−183.
(67) Weller, M. T.; Weber, O. J.; Frost, J. M.; Walsh, A. Cubic Perovskite Structure of Black Formamidinium Lead Iodide, α-$HC(NH_2)_2PbI_3$, at 298 K. *J. Phys. Chem. Lett.* **2015**, *6*, 3209−3212.
(68) East, A. L.; Smith, B. J.; Radom, L. Entropies and Free Energies of Protonation and Proton-Transfer Reactions. *J. Am. Chem. Soc.* **1997**, *119*, 9014−9020.

DOI: 10.1021/acs.jpcc.7b00333
J. Phys. Chem. C 2017, 121, 11977−11984